Bias in boundary layer precipitation parameterizations

ROBERT WOOD[1]

Meteorological Research Flight, The Met. Office, Farnborough, UK

PAUL R. FIELD

Meteorological Research Flight, The Met. Office, Farnborough, UK

WILLIAM R. COTTON

Department of Atmospheric Science, Colorado State University, Fort Collins, USA

ABSTRACT

Due to their large grid-box size, global climate models do not explicitly represent mesoscale processes occurring in cloud systems in the marine boundary layer. One such process, which is thought to have an important climatological effect is the production of warm rain. Parameterizations for this process are generally based around the partitioning of liquid water into a cloud and a rain component. The rate of conversion (autoconversion) of cloud to rain water is expressed as a function of the local liquid water content. It is well known that the distribution of liquid water content within boundary layer cloud systems is spatially non-uniform. The assumption of uniformity is often assumed however, and this results in underprediction of the mean autoconversion rate in the grid box owing to the convex nature of the autoconversion-liquid water content relationship. Here we use aircraft observations to show that the bias in autoconversion can be expressed as a scale-dependent function of the mean liquid water content and that as the length-scale (grid-box size) increases the bias becomes more appreciable. Quantitative values for the bias obtained from FIRE and ASTEX datasets show that, for a given grid-box mean liquid water content, the bias is more significant for ASTEX cloud systems due to the higher variance of liquid water content in these clouds. The autoconversion bias is shown to be a non-scale dependent function of cloud fraction. Suggestions for correction of the bias are presented.

1 Introduction

Boundary layer cloud systems dominate the radiative balance in the subtropics (Slingo 1990). These systems typically extend over millions of square kilometres of ocean and have complex and self-similar structural properties (Lovejoy 1982; Cahalan and Snider 1989). The production of precipitation in marine boundary layer clouds in the subtropics is controlled almost exclusively by warm-rain microphysical processes (condensation, coalescence, sedimentation). Much work has been carried out over the last three decades into the microphysics of warm rain (e.g. see Beard and Ochs 1993 for a brief review). In order to parameterize rainfall in large-scale numerical models many schemes partition the total condensed water into that contained in very small, essentially non-precipitating (cloud) droplets and larger (rain) droplets which dominate the precipitation rate. Rain is produced in these schemes through an autoconversion process (cloud droplets collect each other to form rain drops) and an accretion process (rain drops falling through the cloud collect smaller cloud droplets). The autoconversion process is a local one, insofar as it depends upon local values of the droplet size distribution. It has been shown in a number of studies that the autoconversion rate is very strongly dependent upon the droplet size. For example, Khairoutdinov and Kogan (2000), henceforth KK, used large-eddy simulations with explicit bin microphysics to show that the autoconversion rate is proportional to the droplet mean volume radius (r_{vol}) raised to the power of 5.67. Beheng (1994) also find a very high sensitivity of autoconversion upon droplet size. Therefore, for a constant droplet concentration the autoconversion is strongly dependent upon the liquid water content. For the KK case the autoconversion A, when expressed as a function of liquid water content and droplet concentration was fitted well using

$$A = \left(\frac{\partial q_R}{\partial t}\right)_{auto} = a(N_d)q_C^{\alpha} \tag{1}$$

[1] *Corresponding author address*: Dr. Robert Wood, Meteorological Research Flight, Building Y46, DERA, Farnborough, Hampshire, GU14 6TD, UK
Email: robwood@meto.gov.uk

where a is a function of cloud droplet concentration and alpha is a constant (in the case of KK $\alpha = 2.47$). Similarly, Beheng (1994) found that the autoconversion rate depends very strongly upon the liquid water content. Because these formulas refer to local values of the parameters involved, the question arises as to how to apply them for use in models with large grid-boxes, such as numerical weather prediction and climate models. The application of Jensen's inequality to the problem (Larson et al. 2000) shows that if the grid-box mean liquid water content is used to derive the grid-box mean autoconversion, then (1) always results in an underprediction of the true grid-box mean autoconversion rate providing $\alpha > 1$. This assumes a constant droplet concentration such that the autoconversion depends upon the cloud liquid water content alone. The resulting bias in the calculated gridbox autoconversion rate can be defined as

$$GACB = \frac{\overline{A(q_C)} - A(\overline{q_C})}{\overline{A(q_C)}} \tag{2}$$

where $\overline{A(q_C)}$ is the mean autoconversion calculated from all the values of the liquid water content within the grid-box (the true grid-box mean autoconversion), whereas $A(\overline{q_C})$ is the autoconversion which would be obtained if there was no subgrid variability in the liquid water content. We refer to this bias as the relative grid-box autoconversion bias. Typically, the latter would be calculated in a GCM simulation because currently no information is usually available to allow determination of the subgrid variability. It is also useful to represent the bias as the multiplication factor F that needs to be applied to the calculated $A(\overline{q_C})$ to obtain the unbiased autoconversion rate $\overline{A(q_C)}$:

$$F = \frac{\overline{A(q_C)}}{A(\overline{q_C})} = \frac{1}{1 - GACB}. \tag{3}$$

Pincus and Klein (2000), using hypothetical liquid water content subgrid distributions with properties consistent with observations, show that biases in processes that depend non-linearly upon liquid water content can be as a factor of two. Further, they suggest that the unphysical and undesirable process of tuning GCM parameters so that top-of-atmosphere radiation budgets are balanced, may be necessitated to an extent by the nonaccounting for such biases in GCMs.

The aim of this paper is, first, to use observational data from two campaigns to study subtropical boundary layer clouds to quantify the significance of the autoconversion bias. Second, we use a fractal model of the subgrid variability in the liquid water content to compare with observations. Finally, we propose a method to correct the biases arising from ignorance of the knowledge of the subgrid variability.

2 Observed scale-dependence of bias

Aircraft data used in this study are all taken from *The Met. Office* C-130 research aircraft which flew a total of 21 flights during the First ISCCP Regional Experiment (FIRE, 8 flights; Albrecht et al., 1988) and The Atlantic Stratocumulus Transition Experiment (ASTEX, 13 flights; Albrecht et al., 1995). Details of the thermodynamic instrumentation on the C-130 can be found in Rogers et al. (1995). Microphysical instrumentation is described in Martin et al. (1994). All data presented here are taken from constant-altitude runs in the boundary layer. Cloud fraction was calculated using the method described in Wood and Field (2000).

To compute $GACB$ we choose $\alpha = 2.47$ in Eqn. (1) and substitute into Eqn. (2). The LES model from which the KK parameterization was derived has been validated against observations (Khairoutdinov and Kogan 1999) in stratocumulus cloud. The KK scheme is intended for use as a bulk microphysical parameterization in cloud resolving models but this does not necessarily preclude its use in larger scale models. The parameterization itself has been validated against observational data for a number of drizzling cases (Wood 2000) and was found to behave more favourably than the parameterizations of Kessler (1969), Tripoli and Cotton (1980) and Beheng (1994). We therefore consider the KK parameterization to be the most suitable for describing warm rain precipitation in large-scale numerical models. We examine the bias as a for different values of α in section 3.

To ascertain the scale-dependency of $GACB$ we subdivide the aircraft runs into sub-runs with lengths of 1, 5, 10, 20, 30 and 60 km. All data used were taken at 4 Hz, which at the aircraft speed of 100 m s^{-1}

gives 40 measurements for each kilometre of aircraft track. The GACB is calculated for each sub-run and so for a single 60 km run, the number of subruns will be 2 (30 km), 3 (20 km), 6 (10 km), 12 (5 km) and 60 (1 km) such subruns. The total number of 60 km (or greater) runs used was 103 (FIRE) and 198 (ASTEX). Figure 1 shows an example of $GACB$ values, calculated for the KK scheme, as a function of the run-mean liquid water content q_C. Here, data from all 30 km ASTEX sub-runs are shown. The $GACB$ values here therefore represent the autoconversion bias that would result in a model with no representation of subgrid variability if we assume that the KK scheme has the correct dependency upon local liquid water content. The observed autoconversion bias is largest when the run-mean liquid water content is small and decreases as the liquid water content increases. The reason for this is that with small run-mean liquid water contents, the cloud fraction is likely to be smaller and the largest biases are found when the cloud fraction becomes small. This can be demonstrated using a simple example. Consider that the distribution of cloud within an area is described by regions of clear air and regions of cloudy air with constant liquid water content, and that all the cloudy regions have the same liquid water content q_{cloud}. Let us call this a black-white model (the cloud is either "on" or "off", after Mandelbrot 1983). The total area of cloud is the cloud fraction, C. The in-cloud liquid water content q_{cloud} is given by

$$q_{cloud} = \frac{\overline{q_C}}{C}. \tag{4}$$

where $\overline{q_C}$ is the grid-box mean liquid water content. This is predicted prognostically or diagnostically in large scale numerical models using a variety of cloud schemes (e.g. Smith 1990, Tiedtke 1993, Rotstayn 1997). The autoconversion bias $GACB$ can be calculated using Eqn. (2) and using the substitution Eqn. (4)

$$\begin{aligned} GACB &= \frac{Cq_{cloud}^{\alpha} - (\overline{q_C})^{\alpha}}{Cq_{cloud}^{\alpha}} \\ &= 1 - C^{\alpha-1}. \end{aligned} \tag{5}$$

This simple example shows that in the black-white framework the autoconversion bias is a decreasing function of cloud fraction. Observations (Wood and Field 2000) and cloud resolving model results (Xu and Randall 1996) have shown that the cloud fraction can be expressed as an increasing function of the grid-box mean liquid water content. Hence the observations in Fig. 1 show a behaviour in $GACB$ that is not entirely unlike that of this simple framework. We return to this in the following section.

We found that the observational $GACB$-$\overline{q_C}$ data for each sub-run length L were fitted well using an exponential relation of the form

$$GACB = \exp\left(-\frac{\overline{q_C}}{G(L)}\right) \tag{6}$$

where $G(L)$ is a function of the run length. To calculate the best-fit value of G we minimised *chi*-squared for the difference between the observed $GACB$ and that in Eqn. (6). This also allowed us to calculate errors in the best-fit values of G. The resulting best-fit values of G (assuming $\alpha = 2.47$) are shown in Fig. 2 as a function of sub-run length L for the FIRE and ASTEX datasets. There are two important features:

(i) The function $G(L)$ is larger for ASTEX than for FIRE data;

(ii) The value of $G(L)$ increases with L for both FIRE and ASTEX datasets;

This indicates that for a particular run-mean liquid water content the biases are greater for ASTEX cloud systems than for FIRE ones, and is a result of there being generally greater variability in the liquid water contents in cloud systems typical of ASTEX boundary layers. The relationship can be represented using a power law of the form

$$G = \alpha_G L^{\beta_G} \tag{7}$$

where α_G and β_G are constants for each dataset. Values of α_G calculated from the observations and fractal model are given in Table 1. All errors are quoted at the 95% level. Whilst the values of α_G are clearly different for the ASTEX and FIRE observations, the power exponents β_G are not significantly different at the 95% level (0.32±0.03 for FIRE; 0.29±0.02 for ASTEX). Thermodynamic variability is the ASTEX and FIRE boundary layers is examined in the following section.

We repeat the analysis for several different values of the exponent α in the relationship between local liquid water content and autoconversion rate (Eqn. 1) as there is considerable variability in this exponent in currently used parameterizations. Values for α range from unity (e.g. Kessler 1969, if threshold is set to zero) to 4.7 (Beheng 1994). We choose values of α=1.5, 2.0, 3.0, 4.0, 5.0 to encompass the range of likely dependencies. We do not choose α=1 as a linear relationship does not lead to any bias. For each case we find that the relationship Eqn. 6 reasonably represents the relationship between the autoconversion bias and mean liquid water content. The values of the prefactor α_G and the exponent β_G are derived using chi-squared fitting, for each value of the autoconversion exponent and length scale. Figure 3 shows the derived values of G as a function of length scale and α for FIRE and ASTEX data. The data show that similar scaling is observed for each value of α (i.e. G is approximately proportional to $L^{1/3}$, the gradient of which is denoted by the dashed line in Fig. 3), apart from at $\alpha = 1.5$. We found no significant variation of the exponents β_G for $2 < \alpha < 5$. It is not known why the data for $\alpha = 1.5$ differ from those at higher α, although it is noted that the exponential form (Eqn. 6) does not provide as good a fit to the data at small α.

Figure 4 shows the variation in the prefactor α_G as a function of the autoconversion exponent α for both FIRE and ASTEX. the values of α_G are larger for ASTEX data because of the greater spatial variability in ASTEX cloud systems (see next section). The relationship between α_G and α is approximately linear (the dotted and dashed lines show linear fits).

Figure 5 is a contour plot of the ratio of true to biased autoconversion rate (i.e. $\overline{A(q_C)}/A(\overline{q_C})$) ($\alpha = 2.47$) as a function of both the length scale L and the run-mean liquid water content $\overline{q_C}$. The contours show the factor by which the autoconversion rate calculated using the grid-box mean liquid water content should be multiplied by to give the true grid-box mean autoconversion rate. For a grid-box mean liquid water content of 0.1 g kg^{-1} the ratio increases from around 1.25 to 2.4 for an increase in grid-box size from 10 to 300 km and FIRE-type clouds. It is therefore important that the lengthscale is considered when parameterising the autoconversion bias. However, it will be seen in the following section how the bias, if represented as a function of cloud fraction rather than grid-box mean liquid water content, is almost independent of the grid-box length. However, it is also shown that the relationship between grid-box mean liquid water content and cloud fraction is dependent upon grid-box length because variance in cloud thermodynamic fields increases as the length scale is increased.

3 Bias as a function of cloud fraction

3.1 C<1

Equation (6) describes how the grid-box autoconversion bias changes with run-mean liquid water content. Large eddy simulations from a number of cloud regimes (Cuijpers and Bechtold 1995), from well-mixed stratocumulus-topped to trade-wind cumulus boundary layers, suggest that both cloud fraction C and grid-box mean liquid water content are well modelled as a single function of the normalised saturation deficit Q_1:

$$Q_1 = \frac{a\left(\overline{q_t} - q_{sat}(\overline{T_l})\right)}{\sigma_s} \tag{8}$$

where $\overline{q_t}$ is the grid-box mean total water content and q_{sat} is the saturation specific humidity. Variables in Eqn. 8 are defined as

$$T_l = T - L_e q_C / c_p \tag{9}$$

$$s = a q_t' - b\theta_l' + c \tag{10}$$

$$a = \left(1 + \frac{L_e}{c_p}\left(\frac{\partial q_{sat}}{\partial T}\right)_{T=T_l}\right)^{-1} \tag{11}$$

$$b = a\frac{\overline{T}}{\overline{\theta}}\left(\frac{\partial q_{sat}}{\partial T}\right)_{T=T_l} \tag{12}$$

$$c = a\left(\overline{q_t} - q_{sat}(\overline{T_L})\right) \tag{13}$$

where L_e is the specific heat of vapourisation of water, q_C is the liquid water content, c_p is the specific heat capacity of air at constant pressure and θ_l is the liquid water potential temperature $\theta_l = \theta(1 - L_e q_C/c_p)$.

We validate the LES results of Cuijpers and Bechtold (1995) using aircraft data from FIRE and ASTEX. Figure 6 shows the cloud fraction as a function of the Q_1 for FIRE (filled circles) and ASTEX (triangles). The data presented are taken from the FIRE and ASTEX flights reported in Wood and Field (2000). Most runs were between 50 and 70 km in length. Overplotted are the parameterizations of Cuijpers and Bechtold (dotted line, based upon LES simulations) and the curve obtained for a Gaussian distribution of s. Note that both parameterizations agree fairly well with the observations. It is therefore concluded that the cloud fraction can be obtained to reasonable accuracy given grid-box mean temperature and total water content, provided the standard deviation of the function s is known. We find that σ_s is, in the mean, larger by almost a factor of two for ASTEX data than for FIRE data. We also find that σ_s scales with grid-box size. To examine this we subdivide the aircraft runs into smaller sections (with lengths equal to 1/2, 1/4, 1/8 ... of the original run length) and calculate σ_s for these sub-sections. We then bin the data according to run length and calculate the mean value of σ_s for the dataset. Figure 7 shows the dataset mean values of σ_s as a function of run length L. Error bars represent the standard error in the mean at 95% confidence. Both FIRE and ASTEX exhibit almost identical power law scaling, which can be written

$$\langle\sigma_s\rangle = \alpha_s L^{\beta_s} \tag{14}$$

The fitted values for the exponent β_s are 0.32 $\pm$0.02 (FIRE) and 0.33 $\pm$0.02 (ASTEX). Table 1 shows the scaling If the function s exhibits Kolmogorov ("-5/3") power scaling then the expected value for this exponent would be $\frac{1}{3}$. Because this is close to the observations, this suggests that s follows Kolmogorov-like type of scaling across scales of hundreds of metres to tens of kilometres. The ratio of the standard deviation in ASTEX to that in FIRE is approximately 1.5-1.8 at all scales.

Figure 8 shows observed liquid water content normalised with σ_s plotted against the normalised saturation deficit Q_1. The dashed line represents the relationship obtained from the assumption of Gaussian s. The observed liquid water contents are smaller than the Gaussian ones for Q_1 larger than around 0. The Gaussian model appears to underestimate the liquid water contents at the smallest Q_1. However, observational errors in $\overline{q_C}$ are typically larger when this parameter is small, and so the divergence from the Gaussian model may be an artifact.

Bougeault (1981) shows that for a Gaussian distribution of s, it is possible to write

$$C = \frac{1}{2}\left(1 + \mathrm{erf}(Q_1/\sqrt{2})\right) \tag{15}$$

$$\frac{\overline{q_C}}{\sigma_s} = CQ_1 + \frac{\mathrm{e}^{-Q_1^2/2}}{\sqrt{2\pi}} \tag{16}$$

where erf is the error function. From Eqns. 15 and 16 it is clear that it is possible to express the cloud fraction solely as a function of the ratio of the grid-box mean liquid water content $\overline{q_C}$ to the standard deviation of s. This relationship is shown (solid line) in Fig. 9 together with observations from FIRE (circles) and ASTEX (triangles). The analytic form for the relationship between cloud fraction and normalised liquid water content $\overline{q_C}/\sigma_s$, formed by the combination of Eqns. 15 and 16, is complex. However, it is well parameterized using the exponential form

$$C = 1 - \exp\left(-1.9\frac{\overline{q_C}}{\sigma_s}\right) \tag{17}$$

which is given in Fig. 9 by the dashed line. Given that this exponential form represents a reasonable model for the relationship between mean liquid water content and cloud fraction, we proceed by rearranging Eqn. 17 and substituting $\overline{q_C}$ in Eqn. 6 to give

$$GACB = (1 - C)^{\sigma_s(L)/1.9G(L)} \qquad (C < 1). \tag{18}$$

Thus $GACB$ is a function of cloud fraction C and the potentially scale-dependent function $\sigma_s(L)/G(L)$. Figure 10 shows the values of G plotted against σ_s for three values of α=2.0 (triangles), 3.0 (circles), 5.0 (squares) for FIRE (filled symbols) and ASTEX (open symbols). It is clear that G is well parameterized as a function of σ_s. For each value of α a single relationship exists between σ_s and G for FIRE and ASTEX. It is therefore concluded that the difference in α_G values between FIRE and ASTEX (see Table 1) is a result of differences in variability between the two datasets. Because there is, in general, more variability in ASTEX boundary layers, the values of G (and therefore $GACB$) are generally larger. The three lines are linear fits to the data for each value of α, which may be represented by

$$G(L) = f(\alpha)\sigma_s \tag{19}$$

with $f(\alpha)$ a linear function of α as shown in the inset of Fig. 10, which is found to be given by $f(\alpha) = 1.15(\pm 0.16)(\alpha - 1)$.

The data suggest that it is possible to correct the autoconversion bias if the variance in the boundary layer thermodynamic variable s can be obtained. The boundary layer cloud schemes of Bechtold (1995), Cuijpers and Bechtold (1995) and Lenderink and Siebesma (2000) propose parameterizations of the variance in thermodynamic parameters for use in large scale numerical models. In these schemes the variance is diagnosed as a function of vertical gradients in mean thermodynamic quantities (specific humidity and potential temperature) and turbulence length or velocity scales. This work is a substantial improvement on schemes such as Smith (1990) whose distribution width is a fixed function of temperature and pressure and a critical relative humdidity parameter which is typically a fixed function of height. An improvement to this scheme has been proposed by Cusack et al. (1999) who attempts to predict subgrid variability from resolved information at larger scales.

Substituting equation 19 into 18 gives

$$GACB = (1 - C)^{1/(2.2(\alpha-1))} \tag{20}$$

which leads to a parameterization of $GACB$ as a function only of cloud fraction. For the Khairoutdinov and Kogan (2000) scheme (α=2.47), we obtain the relationship $GACB = (1 - C)^{0.31\pm0.04}$.

As an alternative to proceeding to Eqn. 20 via the exponential relationship Eqn. 6 between mean liquid water and $GACB$, we use the FIRE and ASTEX data to find the best fit between C and $GACB$

$$GACB = (1 - C)^{\gamma}. \tag{21}$$

Thus, to give Eqn. 20, $\gamma = 1/(2.2(\alpha - 1))$. We used *chi*-squared fitting of $GACB$ vs C data to find the values of the exponent γ from the FIRE and ASTEX observations for different sub-run lengths L and found remarkably little dependence of γ upon L, as expected from Eqn. 20. The mean values of γ calculated for the six lengthscales were 0.34±0.02 (FIRE) and 0.35±0.02 (ASTEX), which are only slightly higher than the value predicted using Eqn. 20 and within the margin of error. We therefore conclude that not only is there little or no scale dependence in the parameterisation of $GACB$ as a function of cloud fraction, the same constant γ (approximately 0.34-0.35) is suitable for both FIRE and ASTEX. We carried out the same analysis for different values of α and found that the relationship Eqn. 20 fitted the observed data well.

The observational $GACB$ data ($\alpha = 2.47$) are plotted against cloud fraction in Fig. 11. The parameterizations based upon Eqn. (21) with γ=0.347 (dashed line) and the result of using a black-white model (solid line) are also shown. The former is clearly better, especially at cloud fractions greater than 0.3-0.4. The black-white model, which is often used in GCMs goes a considerable way towards improving the biases in autoconversion.

For models that formulate parameterizations in terms of the black-white model (i.e. those that diagnose an "in-cloud" liquid water content ($= \overline{q_C}/C$), we can calculate an effective bias, which is equal to the ratio of the $GACB$ from Eqn. (21) to that from Eqn. (5). Equvalently, the bias can be expressed in terms of the multiplication factor that would have to be applied to the black-white autoconversion rate to obtain the "true" rate (i.e. that derived from the observations). This factor we call F_{BW} where

$$F_{BW} = \frac{C^{\alpha-1}}{1-(1-C)^{\gamma}}. \quad (22)$$

The curve of F_{BW} against cloud fraction with α=2.47 and $\gamma = 0.347$ is shown in Fig. 12 (solid line with circles). Also shown are the lines obtained using the parameterization $\gamma = 1/(2.2(\alpha-1))$ for values of α from 1.5 to 5.0. For the $\gamma = 0.347$ case, the maximum value of $F_{BW} = 1.74$ occurs at $C = 0.65$. For $C < 0.11$ the black-white model gives a larger bias than the $\gamma = 0.347$ parameterization. As α increases, the black-white model tends to overpredict the autoconversion at increasingly higher cloud fractions. At $C = 1$, $F_{BW} = 1$ which is inconsistent with the observational data for $C = 1$. We suggest that F_{BW} can be used to correct the autoconversion bias when the cloud fraction is less than unity. The problem of parameterizing the bias at $C = 1$ is explored in section 3.2.

3.2 C=1

Both $GACB$ parameterizations above give $GACB = 0$ when $C = 1$, which is clearly a shortcoming. It would be sensible not to use Eqn. (21) when the cloud fraction is approaching unity. We extracted all the observational data with $C > 0.95$ from the datasets and use Eqn. (6) to parameterize $GACB$ as a function of L, using values of G taken from the observational data in Table 1. The parameterized $GACB$ is shown plotted against the observed $GACB$ in Fig. 13 for FIRE and ASTEX. The right and top axes show the parameterized and observed values of the multiplication factor required to correct the autoconversion rate for subgrid variability if the grid-box mean liquid water content is used in Eqn. (1). The parameterization works better for FIRE data than for ASTEX data, with an overprediction of the $GACB$ for larger values for $GACB(observed)$ larger than around 0.15 in the ASTEX dataset. There does not appear to be a significant difference in the location of the data points with different sub-run lengths in Fig. 13 suggesting that the problems with Eqn. (6) in representing the $GACB$ for $C = 1$ for ASTEX are present at all length scales L.

3.3 Summary of suggested parameterization for $GACB$

We propose a method based upon observational and fractal model simulations to correct the bias in autoconversion rate in large-scale numerical models incurred by poor or no treatment of the subgrid variability in liquid water content. In this study, we assume that locally, the autoconversion rate is proportional to the liquid water content to some power α as in Eqn. 1. The autoconversion bias can be formulated either in terms of mean liquid water or cloud fraction:

$$GACB = \begin{cases} (1-C)^{1.0/(2.2(\alpha-1))} & (C < 1 \text{ only}) \\ \exp\left(-\overline{q_C}/G(L)\right) & (\text{all } C) \end{cases} \quad (23)$$

$$\text{where } \; G(L) = 1.15(\alpha-1)\sigma_s \quad (24)$$

with σ_s being a scale dependent function which itself requires parameterization. We do not address the issue of parameterizing σ_s here. It should also be reiterated that this formulation gives the autoconversion bias that a model with absolutely no treatment of subgrid variability will contain. Using Eqns. (23) and (24), the multiplication factor F can be calculated using Eqn. (3); this is applied to the autoconversion rate calculated using the mean liquid water content $A(\overline{q_C})$.

For numerical models which predict cloud fraction and then use the in-cloud liquid water content q_{cloud} calculated using Eqn. (4) to derive the mean autoconversion rate (black-white formulations), we use an effective $GACB$ which takes into account the fact that the black-white formulation accounts for some of the autoconversion bias. In this case, for $C < 1$ we parameterize the multiplication factor F_{BW} which is applied to the calculated autoconversion rate using Eqn. (22). For $C = 1$ the black-white scheme gives $GACB = 0$ and so the parameterization given in Eqns. (23) and Eqns. (24) should be used.

Clearly the parameterization for $C < 1$ does not depend upon the particular cloud regime (i.e. the same equation works for FIRE and ASTEX), but for $C = 1$ a regime-dependent form is required, which raises questions as to which values of $G(L)$ should be used. As stated earlier the differences in $G(L)$ between FIRE and ASTEX result from differences in σ_s between the two regimes. In addition, it is not clear how accurate the parameterization will be for non-boundary layer cloud systems. Rather than presenting a definitive and exhaustive parameterization of the autoconversion bias, this study is aimed (a) highlighting how the autoconversion bias is closely tied to the mean and standard deviation of the distribution of s, and (b) providing a dataset for possible testing of parameterizations of subgrid variability.

4 Discussion and conclusions

Biases in autoconversion rate can arise in large scale models when subgrid variability in liquid water content is ignored. By using aircraft observations from a number of flights during two field programs has allowed us to estimate the magnitude of such biases. We find that the biases increase with increasing run length (equivalent to model grid-box size), and that for the same grid-box mean liquid water content and run length, the mean biases are greater during ASTEX than during FIRE. However, because ASTEX clouds require a higher mean liquid water content than FIRE clouds to achive the same cloud fraction (due to greater variability in ASTEX clouds), it is shown that the bias can be represented as a single function of cloud fraction which is independent of (a) the location (FIRE, ASTEX) and (b) the run length. It is proposed that this behaviour will be useful in attempting to correct the biases. It is also shown how the use of cloud fraction to represent, at least in part, some of the subgridscale variability, removes quite effectively some of the bias. However, when the cloud fraction is unity, this approach can lead to significant biases in autoconversion rate.

The question of how to apply the results presented here to develop better representation of cloud variability is a pertinent one. The observations presented here provide a test-bed for estimates of the autoconversion bias using probability distribution functions to represent the subgrid variability. Future parameterizations which predict subgrid variability from large-scale forcings should be able reproduce the observed differences in grid-box autoconversion bias between the mid-Atlantic (ASTEX) stratocumulus region and the Californian (FIRE) region. Cusack et al. (1999) used model simulations using a relatively small grid-box size to parameterize subgrid variability at larger scales. They found that the spectral power between horizontal scales of 150 km and 400 km varied considerably with location. This novel approach could in future be built upon using nested models which span a wider range of scales from cloud resolving model to climate model grid-box sizes to achieve greater understanding of the physical causes for inhomogeneity. Detailed satellite measurements using a range of sensor resolutions and domain sizes spanning scales from metres to thousands of kilometres have shown that robust scaling relationships exist in nature. Understanding the physical basis for these relationships is a primary goal of future research.

In addition to variability in liquid water content, there is likely to be subgrid variability in droplet concentration due to mesoscale variability in updraught speed and CCN concentration. In this study we have considered that biases in autoconversion result only from heterogeneity in liquid water content. There are physical reasons why droplet concentration may be correlated with liquid water content (or liquid water path), which may result in quite complex biases in autoconversion. In future it also may be possible to represent droplet spectra within a gridbox using a moment scheme such as that presented in Feingold et al. (1998). With schemes such as this, the concepts of autoconversion and accretion are addressed in a more physically realistic manner than by simply partitioning into cloud and rain water. Nevertheless, for large gridbox sizes, neglect of subgrid variability will result in biases; quantifying these biases will be a challenge. The problem of representing subgrid variability in large scale models is likely to be a focus of research for a considerable time to come.

References

Albrecht, B. A., Randall, D. A., and Nicholls, S. N. (1988) Observations of marine stratocumulus during FIRE. *Bull. Am. Meteorol. Soc.*, **69**, 618–626.

Albrecht, B. A., Bretherton, C. S., Johnson, D. W., Schubert, W. H., and Frisch, A. S. (1995) The atlantic stratocumulus transition experiment - ASTEX. *Bull. Am. Meteorol. Soc.*, **76**, 889–904.

Beard, K. V., and Ochs H. T., (1993) Warm-rain initiation: An overview of microphysical mechanisms. *J. Appl. Meteorol.*, **32**, 608–625.

Bechtold, P., Cuijpers, J. W. M., Mascart, P., and Trouilhet, P. (1995) Modelling of trade wind cumuli with a low-order turbulence model: toward a unified description of Cu and Sc clouds in meteorological models. *J. Atmos. Sci.*, **52**, 455–463.

Beheng, K. D., (1994) A parameterization of warm cloud microphysical processes. *Atmos. Res.*, **33**, 193–206

Cahalan, R. F., and Snider, J. B., (1989) Marine stratocumulus structure. *Remote Sens. Environ.*, **28**, 95–107.

Cuijpers, J. W. M., and Bechtold, P. (1995) A simple parameterization of cloud water related variables for use in boundary layer models. *J. Atmos. Sci.*, **52**, 2486–2490.

Cusack, S., Edwards, J. M, and Kershaw, R., (1999) Estimating the subgrid variance of saturation, and its parametrization for use in a GCM cloud scheme. *Quart. J. Roy. Meteorol. Soc.*, **125**, 3057–3076.

Feingold, G., Walko, R. L., Stevens, B., and Cotton, W. R., (1998) Simulations of marine stratocumulus using a new microphysical parametrization scheme. *Atmos. Res.*, **47-48**, 505–528.

Kessler, E., (1969) On the distribution and continuity of water substance in atmospheric circulations. *Meteor. Monogr.*, **32**, Amer. Meteorol. Soc., 1-84.

Khairoutdinov, M. and Kogan, Y. L., (2000) A new cloud physics parametrization in a large-eddy simulation model of marine stratocumulus. *Mon. Wea. Rev.*, **128**, 229–243.

Khairoutdinov, M. and Kogan, Y. L., (1999) A large eddy simulation model with explicit microphysics: validation against aircraft observations of a stratocumulus-topped boundary layer. *J. Atmos. Sci.*, **56**, 2115–2131.

Larson, V. E., Wood, R., Field, P. R., Golaz, J.-C., Vonder Haar, T. H., and Cotton, W. R., (2000) Systematic biases in the microphysics and thermodynamics of numerical models that ignore subgrid-scale variability. Submitted to *J. Atmos. Sci.*, November 1999.

Lenderink, G., and Siebesma, A. P. (2000) Combining the massflux approach with a statistical cloud scheme. *Proceedings of the 14th Symposium on Boundary Layers and Turbulence*, Aspen, Colorado, USA, 7-11 August, 2000.

Lovejoy, S., (1982) Area-perimeter relation for rain and cloud areas. *Science*, **216**, 185-187.

Mandelbrot, B., (1983) *The Fractal Geometry of Nature.* W. H. Freeman, New York, 460pp.

Martin, G. M., Johnson, D. W., Rogers, D. P., Jonas, P. R., Minnis P., and Hegg, D. A. (1995) Observations of the interaction between cumulus clouds and warm stratocumulus in the marine boundary layer during ASTEX, *J. Atmos. Sci.*, **52**, 2902–2922.

Pincus, R., and Klein, S. A., (2000) Unresolved spatial variability and microphysical process rates in large scale models. Submitted to *J. Geophys. Res.*, April 2000.

Rogers, D. P., Johnson, D. W., and Friehe, C. A. (1995) The stable internal boundary layer over a coastal sea. Part I: Airborne measurements of the mean and turbulence structure. *J. Atmos. Sci.*, **52**, 684–696.

Rotstayn, L. D., (1997) A physically based scheme for the treatment of stratiform clouds and precipitation in large scale models. *Quart. J. Roy. Meteorol. Soc.*, **123**, 1227–1282.

Slingo, A. (1990) Sensitivity of the earth's radiation budget to changes in low clouds. *Nature*, **343**, 49–51.

Smith, R. N. B. (1990) A scheme for predicting layer clouds and their water content in a general circulation model. *Quart. J. Roy. Meteorol. Soc.*, **116**, 435–460.

Tiedtke, M. (1993) Representation of clouds in large-scale models. *Mon. Wea. Rev.*, **121**, 3041-3061.

Tripoli, G. J. and Cotton, W. R., (1980) A numerical investigation of several factors contributing to the observed variable intensity of deep convection of south Florida. *J. Appl. Meteorol.*, **19**, 1037–1063.

Xu, K-M. and Randall, D. A. (1996) A semiempirical cloudiness parameterization for use in climate models. *J. Atmos. Sci.*, **53**, 3084–3102.

Wood, R., and Field, P. R. (2000) Relationships between total water, condensed water and cloud fraction examined using aircraft data. *J. Atmos. Sci.*, **57**, 1888–1905.

Wood, R. (2000) The validation of drizzle parametrizations using aircraft data. *Proceedings of the 13th International Conference on Clouds and Precipitation*, Reno, Nevada, USA, 14-18 August 2000.

Tables

Table 1: *GACB* scaling parameters derived from the corrected observations and the fractal model.

Dataset	α_G [g kg^{-1}]	β_G	α_s [g kg^{-1}]	β_s
FIRE (obs)	0.045±0.005	0.32±0.03	0.028±0.001	0.32±0.02
ASTEX (obs)	0.084±0.003	0.29±0.02	0.050±0.002	0.33±0.02

Figure captions

Figure 1. Example of relationship between $GACB$ and run-mean liquid water content $\overline{q_C}$. Observational data from runs of length 30 km from ASTEX is shown. It is clear that the autoconversion bias decreases with increasing run-mean liquid water content and is fitted reasonably well using a relation of the form $GACB$ =exp($-G\overline{q_C}$) (dashed line). The exponential was fitted by minimising *chi*-squared differences between the observed and parameterized $GACB$.

Figure 2. Best fit grid box autoconversion bias parameter G as a function of sub-run length L for the FIRE (solid circles) and ASTEX (open triangles) datasets. The error bars represent the 95% confidence intervals calculated using *chi*-squared fitting of observational data. The dotted and dashed lines are the results from a multiplicative cascade model (see text for details) for FIRE (dotted) and ASTEX (dashed), with 95% confidence limits for each shown by the thin solid lines.

Figure 3. Values of G plotted against run length scale L for different values of the exponent α relating local liquid water content to autoconversion rate. The values of G were derived from the data using chi-squared fitting of $\overline{q_C} - GACB$ data. Both FIRE data (left panel) and ASTEX data (right panel) exhibit quite well-defined power law scaling - the dashed line has a power law scaling of $L^{1/3}$, apart from the data for $\alpha = 1.5$. It is uncertain why the power law scaling at $\alpha = 1.5$ is different.

Figure 4. Values of the prefactor α_G (Eqn. 6) against the autoconversion exponent α for FIRE (circles) and ASTEX (triangles) data. There is no bias (hence $\alpha_G = 0$) when the local liquid water content and autoconversion rate are linearly related ($\alpha = 1$). The dotted and dashed lines represent straight line fits to the data passing through point ($\alpha = 1;\alpha_G = 0$). The ratio of the gradients of the ASTEX and FIRE fits is approximately 1.6.

Figure 5. Contour plot showing ratio of the true grid-box mean autoconversion rate ($\overline{A(q_C)}$) to the biased autoconversion rate $A(\overline{q_C})$ as a function of lengthscale and liquid water content for FIRE (solid contours) and ASTEX (dotted contours). The value of $\alpha = 2.47$, in accordance with the formulation of Khairoutdinov and Kogan (2000). The observed scaling parameters α_G and β_G were used to compute the contours.

Figure 6. Cloud fraction from observations (circles, FIRE; triangles, ASTEX) plotted against Q_1 defined in Equation 8. Also shown are the proposed parameterization of Cuijpers and Bechtold (C+B 95, dotted line) based upon LES results, and the relationship obtained if a Gaussian distribution of s is assumed (dashed line). The observations agree well with LES-derived results. The Gaussian assumption also provides a good fit to the observational data.

Figure 7. Dataset mean values of σ_s for FIRE (circles) and ASTEX (triangles) observations as a function of run length L. The dotted and dashed lines are power law fits to the FIRE and ASTEX data respectively. The solid line shows the (1/3) power law expected if s follows a (-5/3) power spectral scaling.

Figure 8. Mean liquid water content normalised with σ_s plotted against Q_1 for FIRE and ASTEX data. The dashed line shows the relationship corresponding to the Gaussian distribution of s.

Figure 9. Cloud fraction against mean liquid water content normalised with σ_s for FIRE (circles) and ASTEX (triangles). Assuming a Gaussian distribution of s gives the solid line, which is itself well parameterized by a more simple exponential form (dashed line, Eqn. 9).

Figure 10. Plot of σ_s against G from FIRE (filled symbols) and ASTEX (open symbols). Data are only shown for α=2.0 (triangles), 3.0 (circles) and 5.0 (squares). Lines are linear fits to data for each value of α. The gradient of these fits $f(\alpha)$ is plotted as a function of α in the inset.

Figure 11. Plot of grid-box autoconversion bias against cloud fraction for FIRE (solid circles) and ASTEX (open triangles) data. Data are averaged into bins and the error bars represent the error in the mean value in that bin. The parameterisation for the black-white (constant in-cloud liquid water content) model of Eqn. (5) with $\alpha = 2.47$ is shown (solid line) along with the curve representing the best fit to the $C - GACB$ data ($\gamma = 0.347$, dashed line) and the parameterization derived from Eqn.

(20) (dotted line). A Gaussian distribution of s results in the curve shown by the dash-dot line.

Figure 12. Multiplication correction factor F_{BW} for correcting black-white model to give mean autoconversion rates parameterized using observational data for FIRE and ASTEX, plotted as a function of the cloud fraction. The different lines represent different values of α ranging from 1.5 (solid line) to 5.0 (long dash). The circle-solid line represents the best fit parameterization derived directly from the $C - GACB$ data - all other lines are derived from the exponential relationship between liquid water content and $GACB$.

Figure 13. Observed $GACB$ for FIRE (top) and ASTEX (bottom) against that parameterized using Eqn. (6) and $G(L)$ from the power law Eqn. (7) with observed values of the parameters in Table 1. Different sub-run lengths are given different symbols as shown in the key. The right and top axes in each figure show, respectively, the parameterized and observed values of F, the multiplication factor required to obtain the true grid-box mean autoconversion rate.

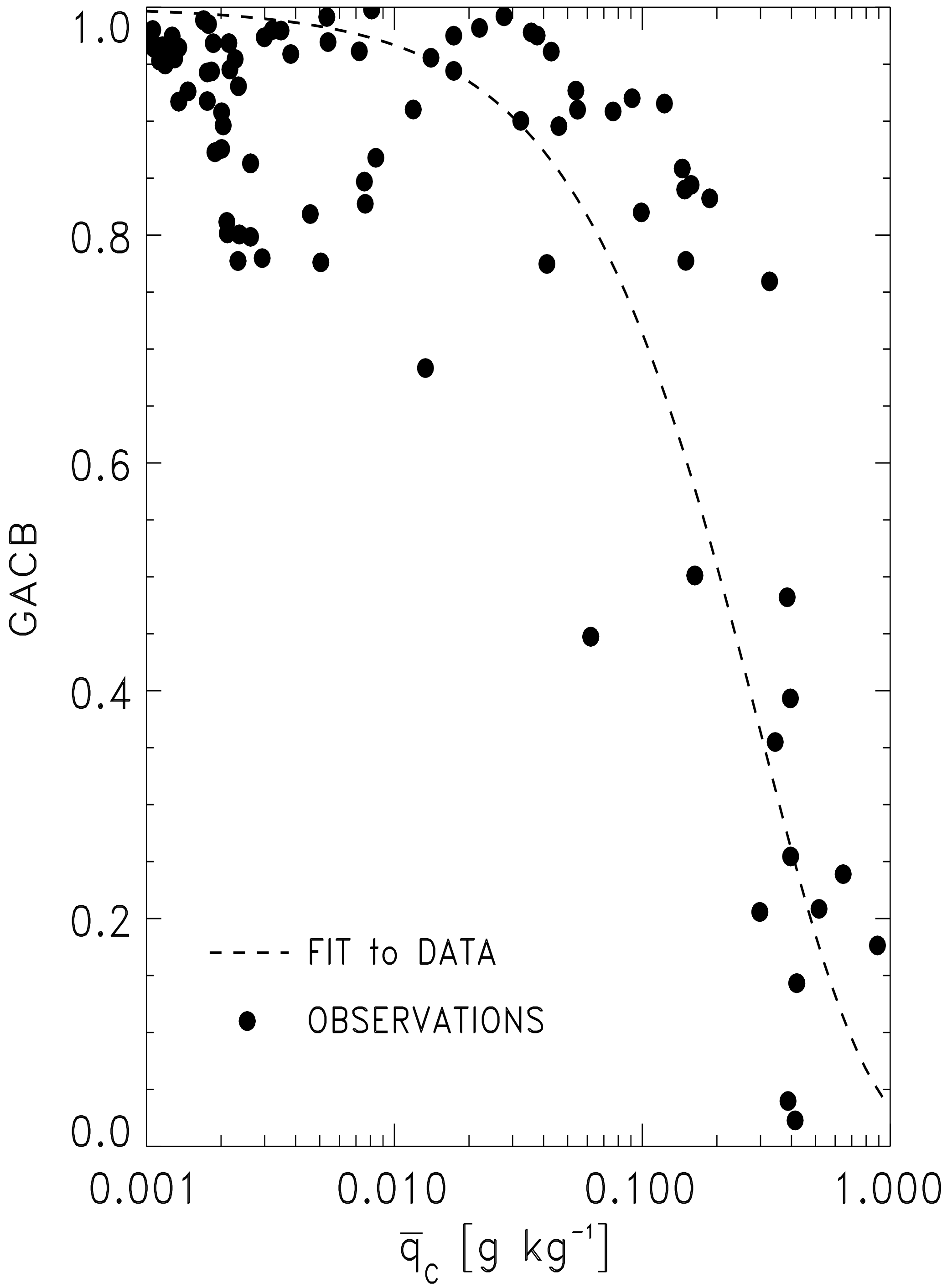
1.0
0.8
0.6
0.4
0.2
0.0
GACB
0.001
0.010
0.100
1.000
$\overline{q}_c$ [g kg^{-1}]
FIT to DATA
OBSERVATIONS

Figure 1:

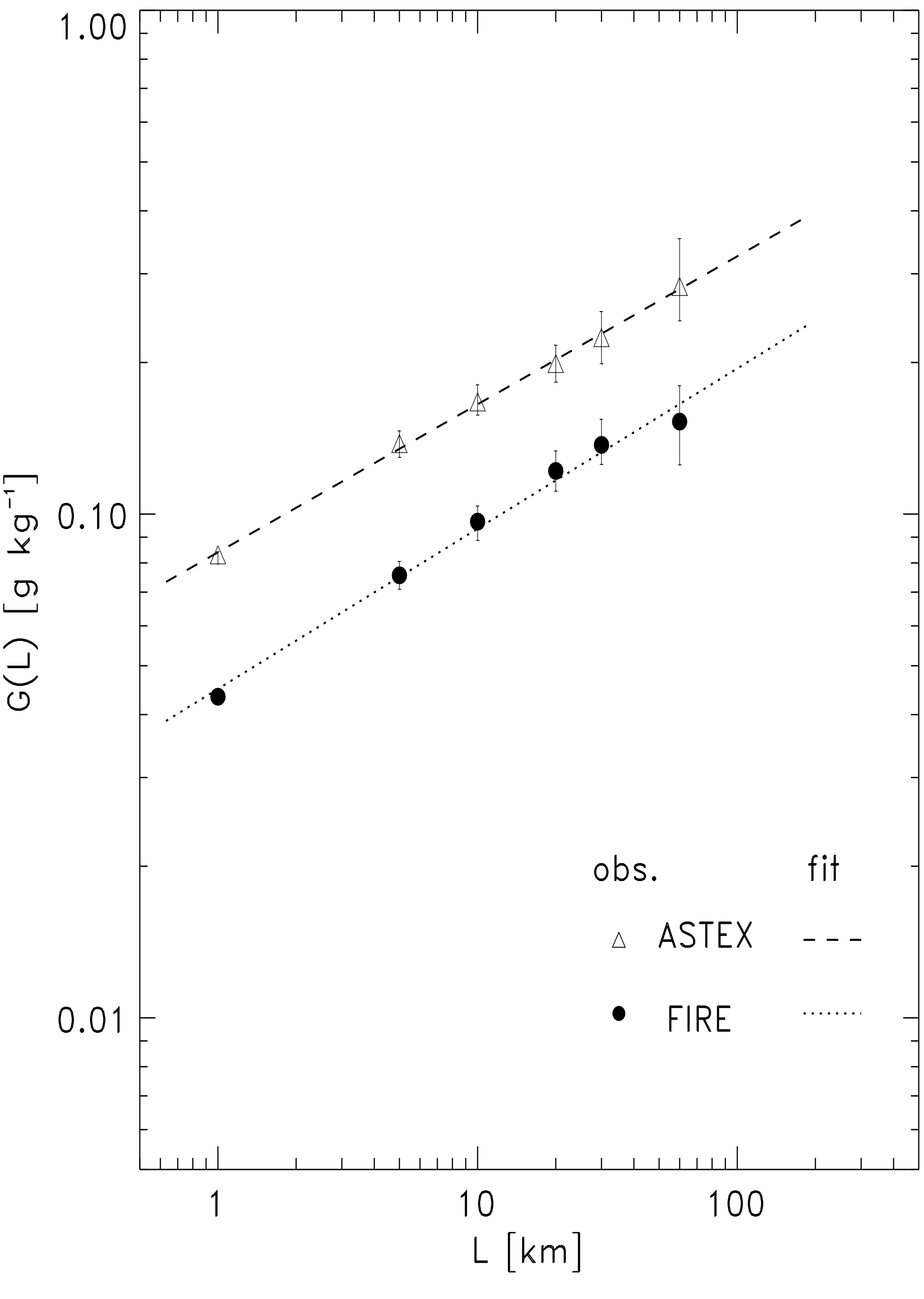

Figure 2:

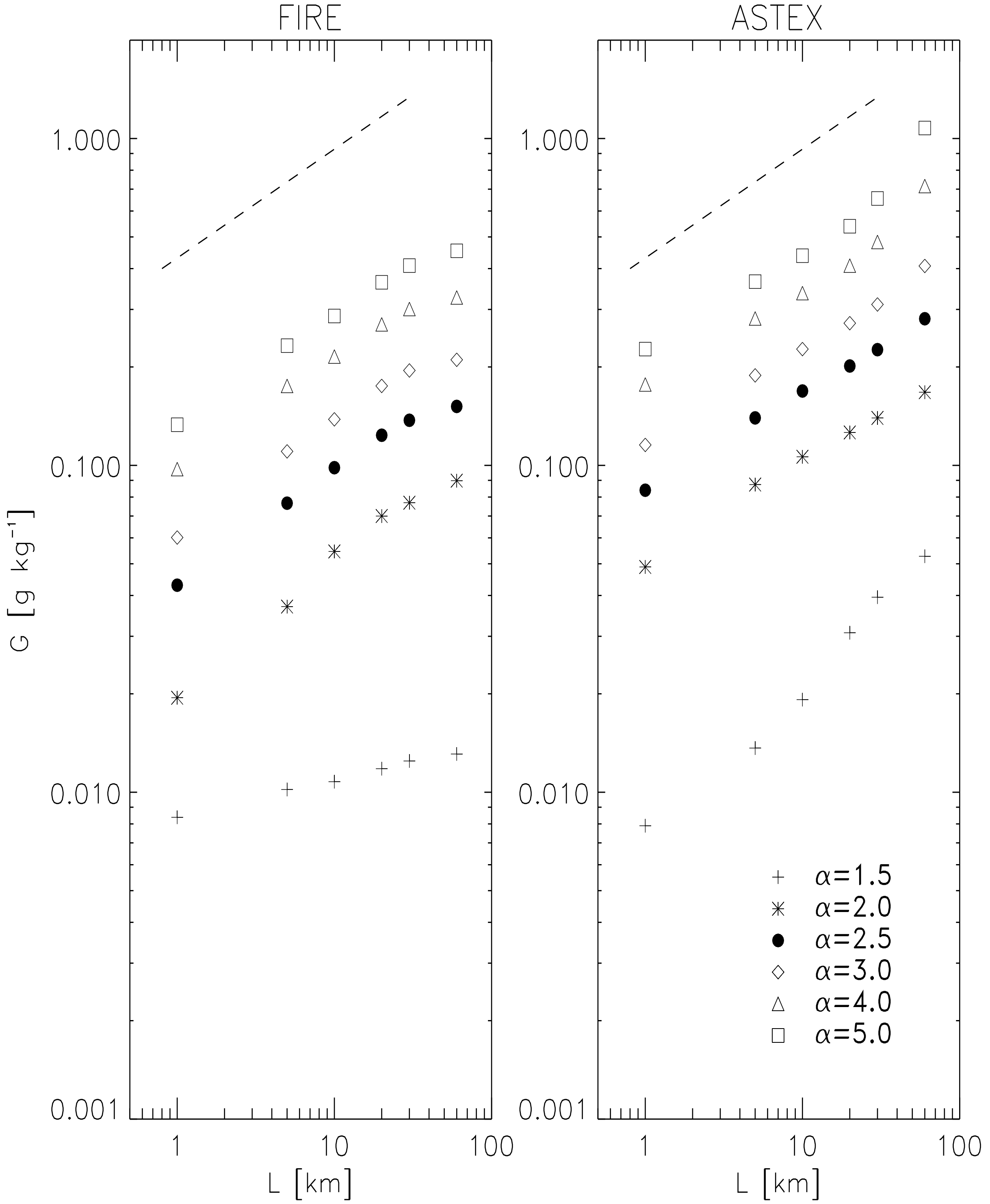
FIRE
ASTEX
G [g kg⁻¹]
L [km]
1.000
0.100
0.010
0.001
1
10
100
α=1.5
α=2.0
α=2.5
α=3.0
α=4.0
α=5.0

Figure 3:

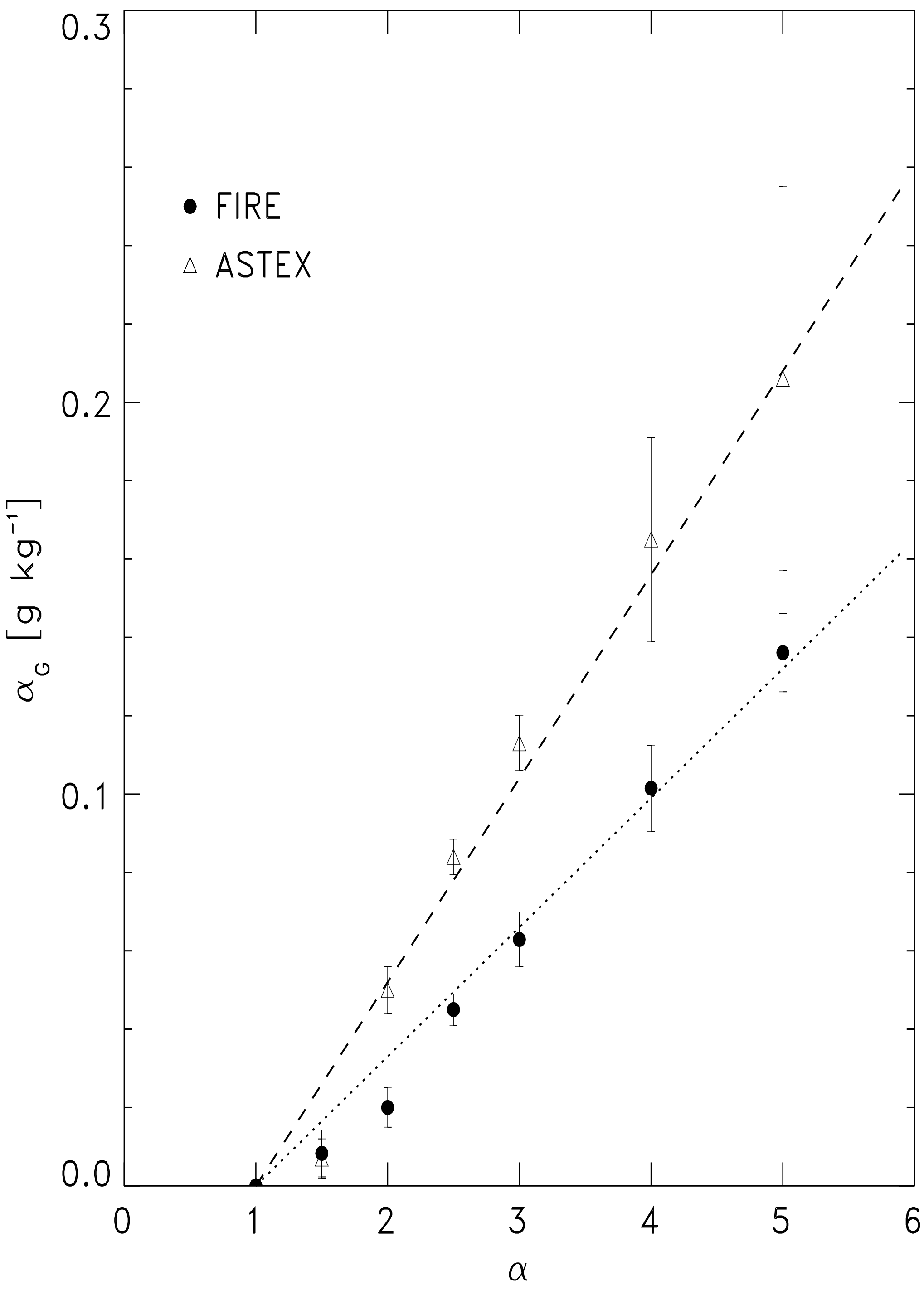

Figure 4:

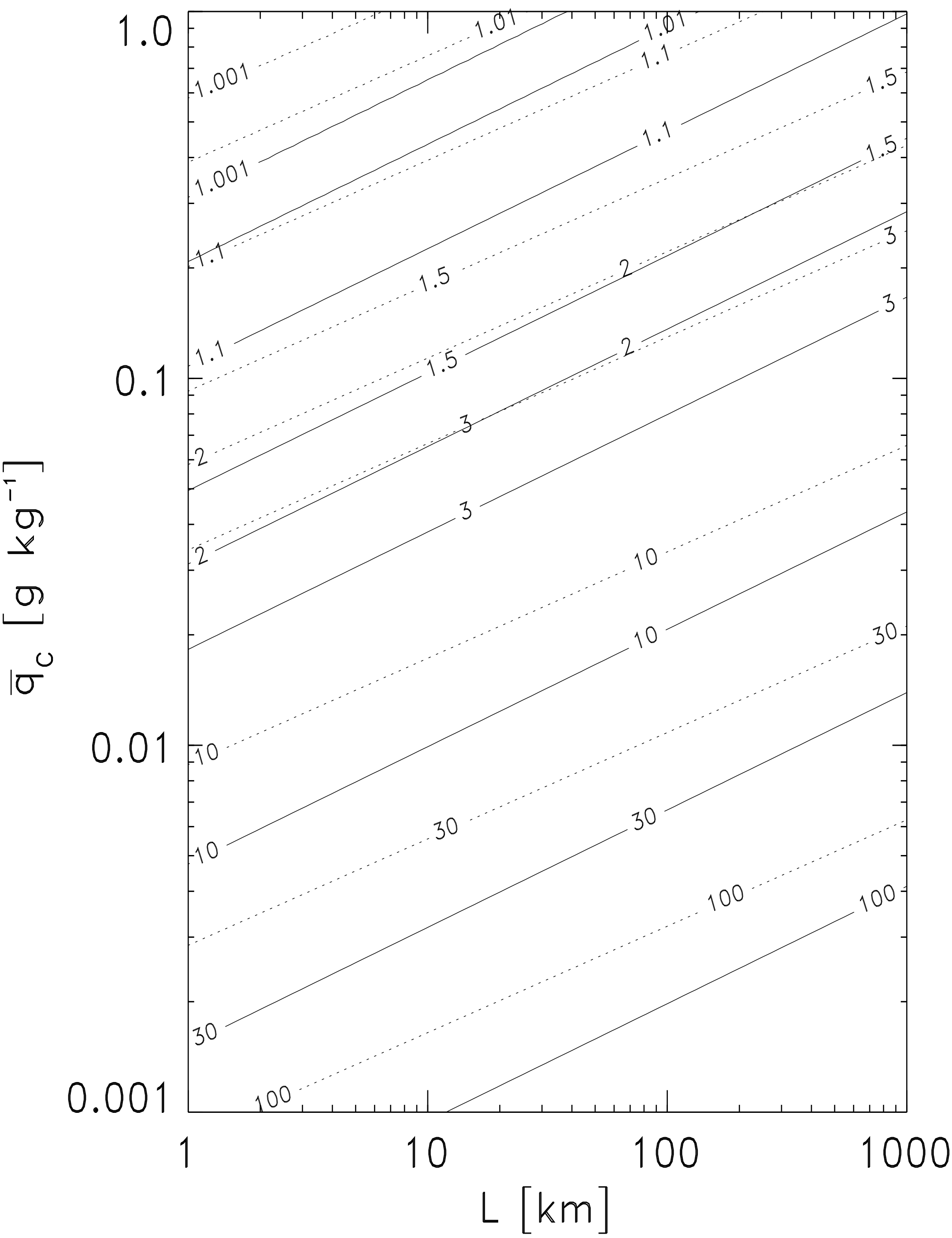
1.0
0.1
0.01
0.001
1
10
100
1000
L [km]
$\bar{q}_c$ [g kg^{-1}]
1.001
1.01
1.1
1.5
2
3
10
30
100

Figure 5:

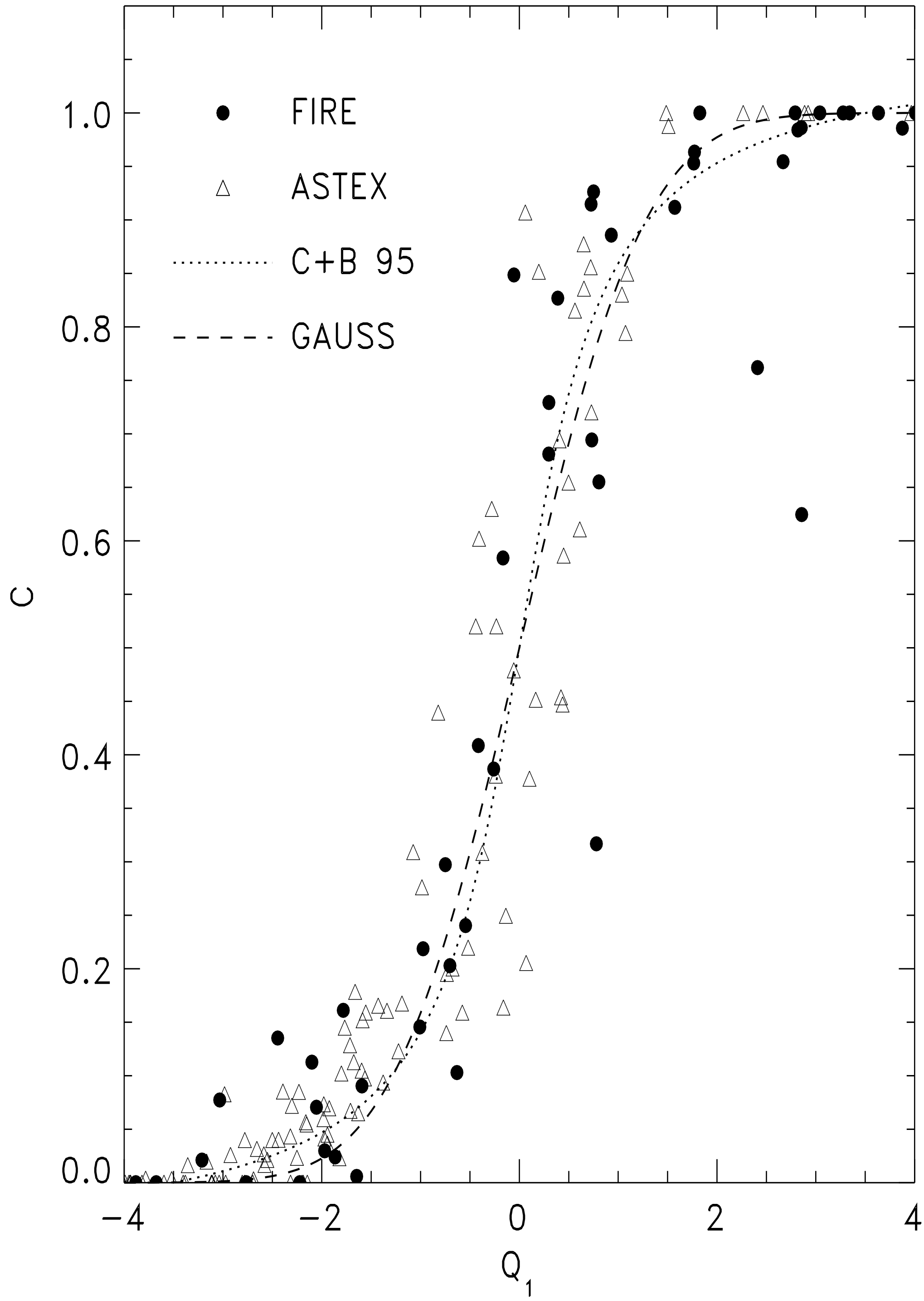

Figure 6:

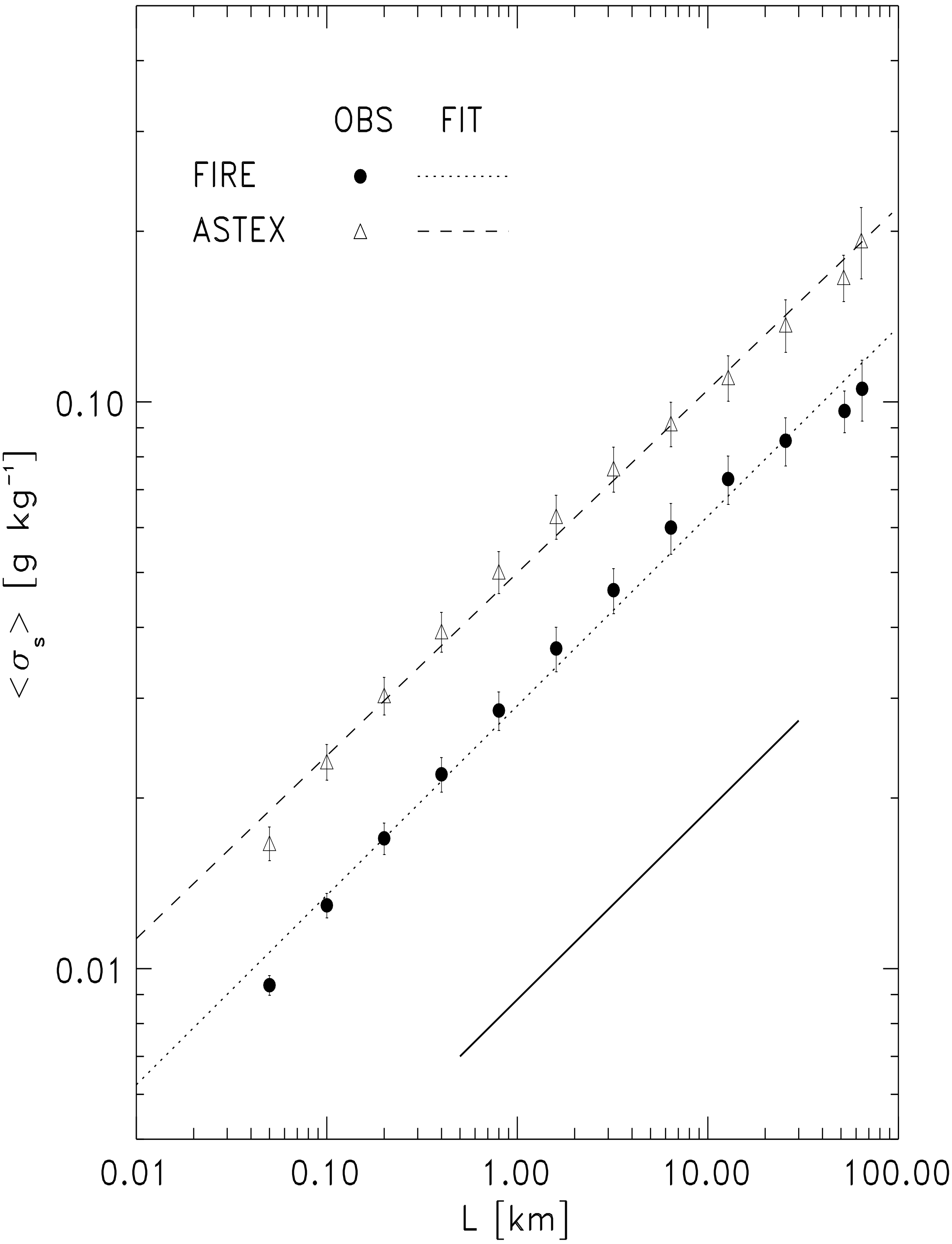

OBS FIT
FIRE
ASTEX
0.10
0.01
$\langle\sigma_s\rangle$ [g kg^{-1}]
0.01
0.10
1.00
10.00
100.00
L [km]

Figure 7:

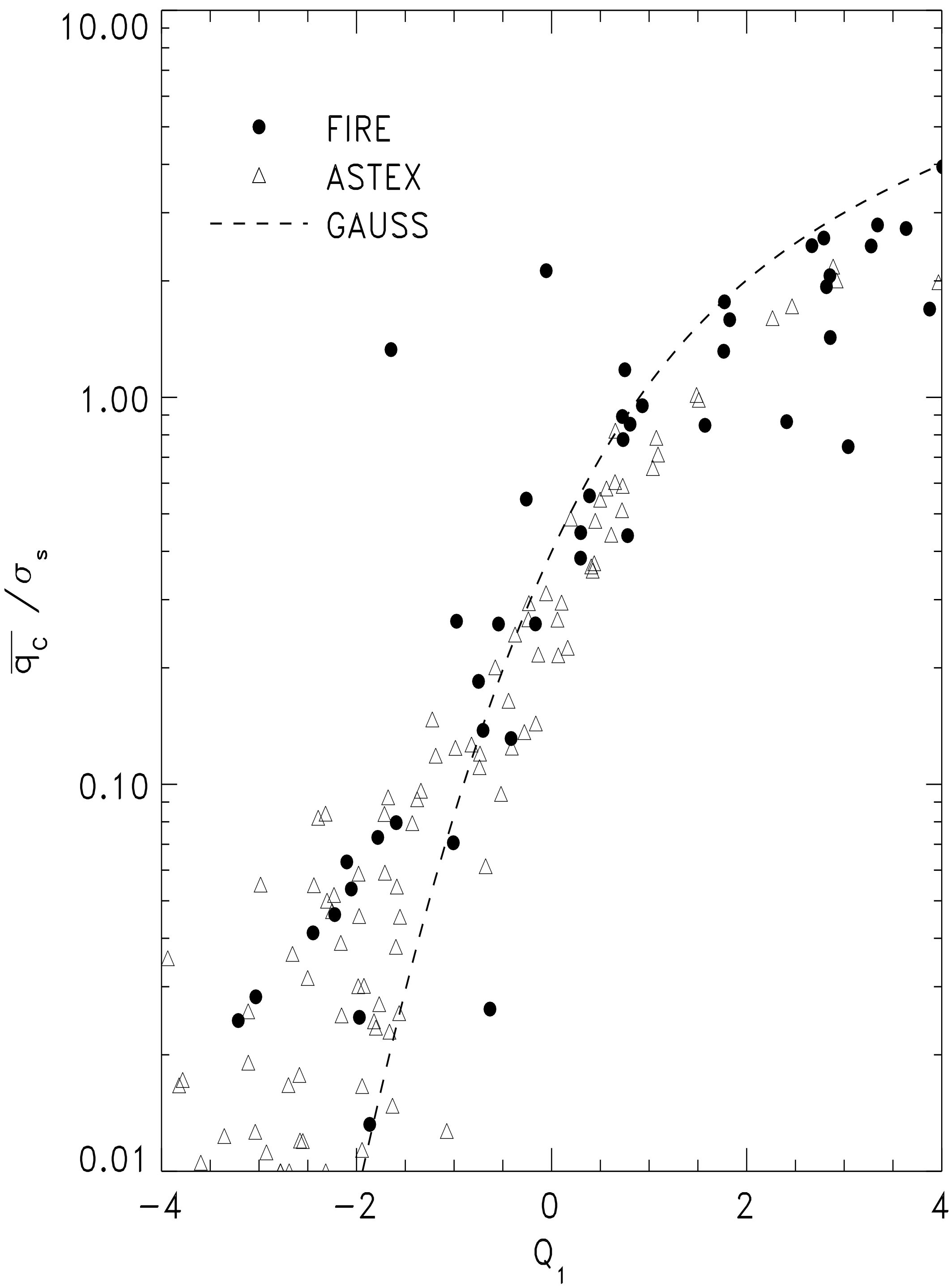
10.00
1.00
0.10
0.01
FIRE
ASTEX
GAUSS
$\overline{q_c}\ /\sigma_s$
−4
−2
0
2
4
Q_1

Figure 8:

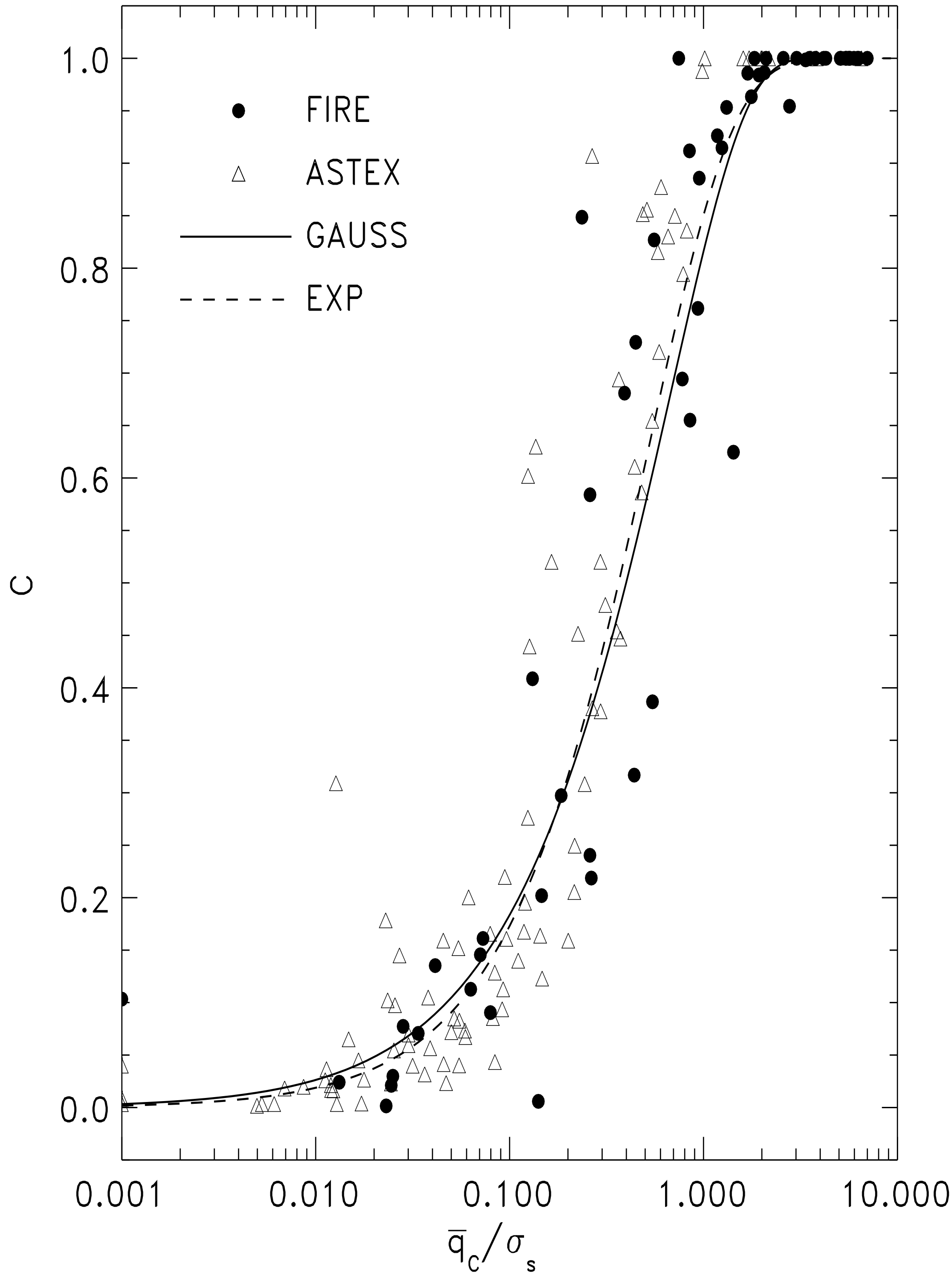
1.0
0.8
0.6
0.4
0.2
0.0
C
FIRE
ASTEX
GAUSS
EXP
0.001
0.010
0.100
1.000
10.000
$\overline{q}_c/\sigma_s$

Figure 9:

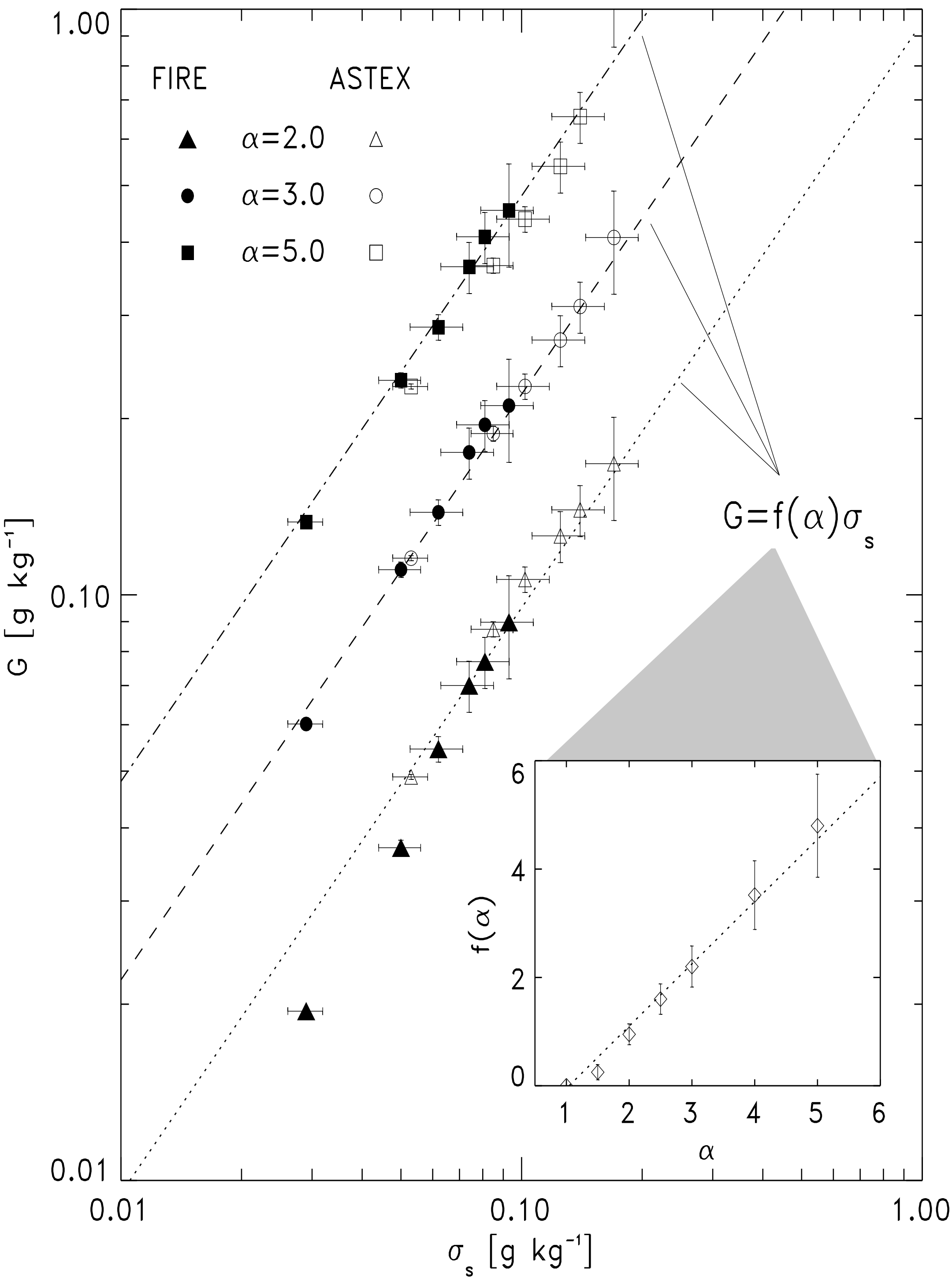
1.00
0.10
0.01
G [g kg⁻¹]
0.01
0.10
1.00
σ_s [g kg⁻¹]
FIRE
ASTEX
α=2.0
α=3.0
α=5.0
G=f(α)σ_s
f(α)
α
0
2
4
6
1
2
3
4
5
6

Figure 10:

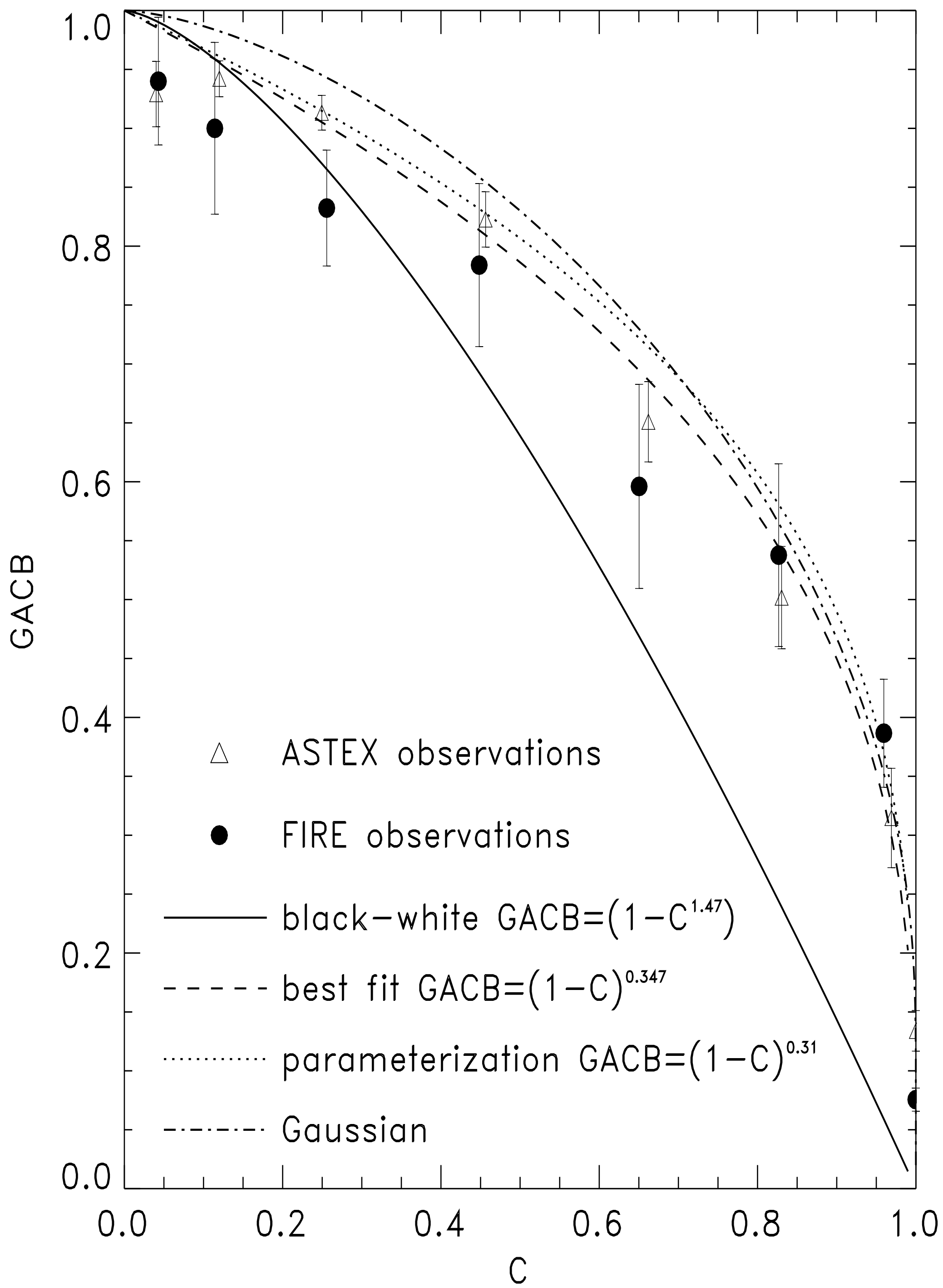
1.0
0.8
0.6
0.4
0.2
0.0
GACB
0.0
0.2
0.4
0.6
0.8
1.0
C
ASTEX observations
FIRE observations
black-white GACB=$(1-C^{1.47})$
best fit GACB=$(1-C)^{0.347}$
parameterization GACB=$(1-C)^{0.31}$
Gaussian

Figure 11:

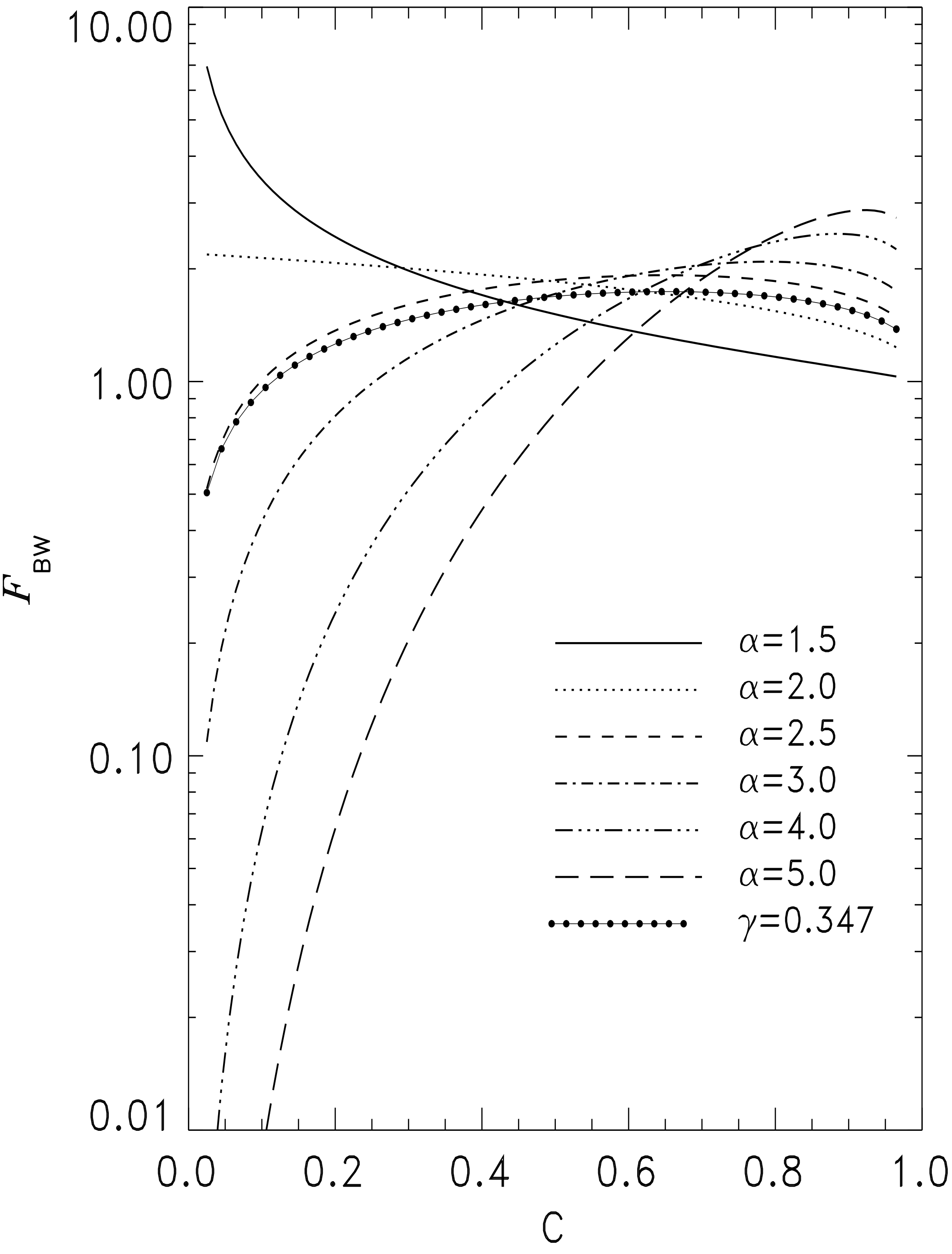

10.00
1.00
0.10
0.01
0.0
0.2
0.4
0.6
0.8
1.0
F_{BW}
C
α=1.5
α=2.0
α=2.5
α=3.0
α=4.0
α=5.0
γ=0.347

Figure 12:

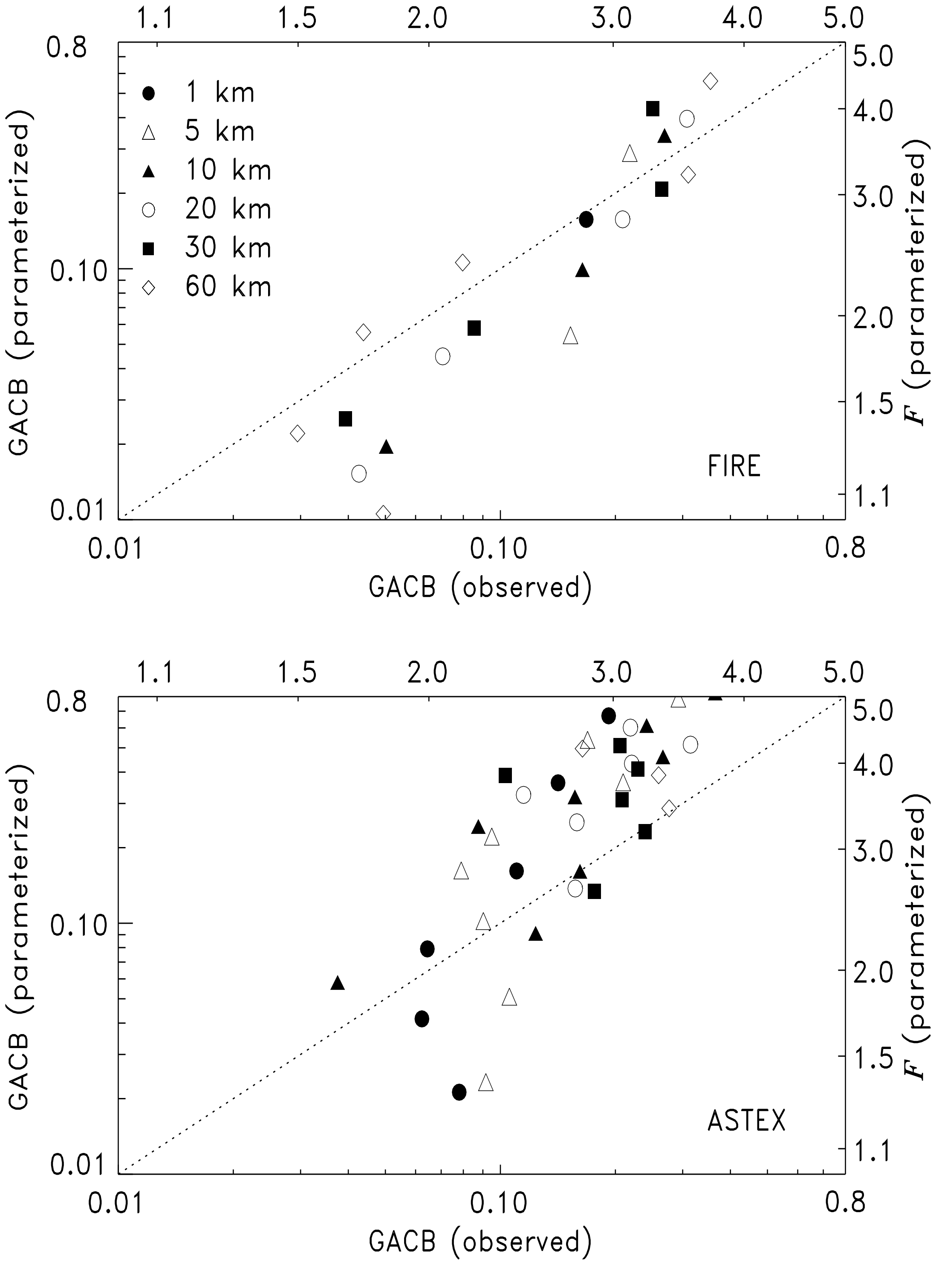
1.1
1.5
2.0
3.0
4.0
5.0
0.8
0.10
0.01
1 km
5 km
10 km
20 km
30 km
60 km
GACB (parameterized)
F (parameterized)
FIRE
0.01
0.10
0.8
GACB (observed)
ASTEX

Figure 13: